[I]

Two-stage reconstruction of a circular anomaly in electrical impedance tomography

Sampsa Pursiainen

Inverse Problems.
Vol. 22(5), pp. 1689–1703, 2006.

http://www.iop.org/journals/ip
http://stacks.iop.org/ip/22/1689

INSTITUTE OF PHYSICS PUBLISHING INVERSE PROBLEMS

Inverse Problems **22** (2006) 1689–1703 doi:10.1088/0266-5611/22/5/010

Two-stage reconstruction of a circular anomaly in electrical impedance tomography

Sampsa Pursiainen

Institute of Mathematics, Box 1100, FI-02015 Helsinki University of Technology, Finland

E-mail: Sampsa.Pursiainen@hut.fi

Received 7 December 2005, in final form 18 May 2006
Published 30 August 2006
Online at stacks.iop.org/IP/22/1689

Abstract

In the electrical impedance tomography inverse problem, an unknown conductivity distribution in a given object is to be reconstructed from a set of noisy voltage measurements made on the boundary. This paper focuses on the development of effective reconstruction techniques for detection of a circular anomaly from an otherwise constant background. The goal is to investigate applicability of a two-stage reconstruction process in which a region of interest (ROI) containing the anomaly (e.g. a tumour) is determined in the first stage, and the actual reconstruction is found in the second stage by exploring the ROI. Bayesian inversion methods are applied. The conductivity distribution is modelled as a random variable that follows a posterior probability density proportional to the product of a prior density and a likelihood function. The investigated two-stage reconstruction strategy is, however, not fully Bayesian. In the first stage, the ROI is determined using a quasi-Newton optimization algorithm and a smoothness prior, and in the second stage, the reconstruction is found using Markov chain Monte Carlo sampling and an anomaly prior. Performances of white noise and enhanced noise models as well as performances of standard and linearized finite element forward simulations are compared.

(Some figures in this article are in colour only in the electronic version)

1. Introduction

In electrical impedance tomography (EIT), an unknown conductivity distribution σ in an object Ω is reconstructed from noisy voltage measurement data given on the boundary $\partial\Omega$. This is a nonlinear and an ill-conditioned inverse problem: small errors in voltage measurements or in forward modelling can lead to very large fluctuations in the reconstructions. The problem was first introduced in a rigorous mathematical form in 1980 by Calderón [4]. At present, applications of EIT are numerous. These include detection and classification of tumours in

0266-5611/06/051689+15$30.00

breast tissue [8, 13, 19, 21, 33], measuring brain function [9, 23], imaging of fluid flows in process pipelines [10, 14, 27, 29], and non-destructive testing of materials [18, 32]. EIT has been reviewed by Cheney *et al* [7].

This paper focuses on the development of effective reconstruction techniques for detection of a circular anomaly from an otherwise constant background. The goal is to investigate a two-stage reconstruction process in which a region of interest (ROI) potentially containing the anomaly is determined in the first stage, and the final reconstruction is found in the second stage by exploring the ROI. This approach is investigated regarding clinical applications, such as detection of a tumour in breast tissue, in which the ROI can be decided based on a diagnosis by an expert. Anomalous conductivities in EIT have been considered in many studies [1–3].

Bayesian inversion methods are applied. The unknown conductivity distribution is modelled as a random variable that follows a posterior probability density proportional to the product of a likelihood function and a prior density, which contains *a priori* knowledge of conductivity distribution. The investigated two-stage reconstruction strategy is, however, not fully Bayesian. In the first stage, the ROI is determined using a quasi-Newton optimization algorithm and a smoothness prior, and in the second stage, the reconstruction is found using Markov chain Monte Carlo (MCMC) sampling and an anomaly prior based on the ROI. Quasi-Newton algorithms are traditional reconstruction methods in EIT. MCMC sampling, proposed by Fox and Nicholls [11], is commonly used at present. For a review of these methods, see Kaipio *et al* [16].

This paper is organized as follows. The reconstruction problem is briefly reviewed in section 2. The two-stage reconstruction process, forward simulation methods, constructions of the priors and reconstruction algorithms are described in section 3. Section 4 reports the numerical experiments. Finally, section 5 summarizes the results and discusses possible directions for the future work.

2. EIT inverse problem

In the present version of electrical impedance tomography, a number of current patterns of the form $I = (I_1, I_2, \ldots, I_L)$ are injected into a two- or three-dimensional domain Ω through a set of contact electrodes $e_1, e_2, \ldots, e_L$ attached to the boundary $\partial\Omega$. An injected current pattern induces a potential field u in the domain and voltages $U_1, U_2, \ldots, U_L$ on the electrodes. A vector that contains all the induced electrode voltages stacked together is denoted by $\mathbf{U}$. Voltage data are gathered by measuring these voltages. The measurements are contaminated by noise. A vector containing the noisy voltage data is denoted by $\mathbf{V}$.

2.1. Complete electrode model

In the *complete electrode model* (CEM), the contact impedance between the electrode e_ℓ and the boundary is characterized by $z_\ell > 0$. The electrode voltages U induced by the current pattern I can be found by solving the *forward problem* described by the equation

$$\nabla \cdot (\sigma \nabla u) = 0 \qquad \text{in} \quad \Omega,$$

under the boundary conditions

$$\sigma \frac{\partial u}{\partial n}\bigg|_{\partial\Omega \setminus \cup_\ell e_\ell} = 0, \qquad \int_{e_\ell} \sigma \frac{\partial u}{\partial n}\, \mathrm{d}s = I_\ell, \qquad \left(u + z_\ell \sigma \frac{\partial u}{\partial n}\right)\bigg|_{e_\ell} = U_\ell, \quad (1)$$

with $\ell = 1, 2, \ldots, L$, and by Kirchoff's current and voltage laws $\sum_{\ell=1}^{L} I_\ell = 0$, $\sum_{\ell=1}^{L} U_\ell = 0$. According to Somersalo *et al* [28], under certain assumptions made on the domain and on

the conductivity distribution, the weak form of the forward problem has an existing unique solution $(u, U) \in H^1(\Omega) \oplus \mathbb{R}^L$. Consequently, the CEM equations describe a nonlinear *forward map* $\sigma \to \mathbf{U}(\sigma)$ from the set of all admissible conductivities $\mathcal{A}$ to the set of all possible noiseless electrode voltage vectors [16].

2.2. Bayesian inversion

The reconstruction problem can be formulated through the classical Bayes formula

$$p(\sigma|\mathbf{V}) = \frac{p(\sigma)p(\mathbf{V}|\sigma)}{p(\mathbf{V})}.$$

The probability density $p(\sigma)$, supported on the set of admissible conductivities $\mathcal{A}$, is the prior density that contains *a priori* information about the conductivity distribution, and $p(\mathbf{V}|\sigma)$ is the likelihood that is the conditional density of measuring $\mathbf{V}$. For given measurement data, the product of the prior and the likelihood constitutes the posterior density $p(\sigma|\mathbf{V})$ up to a constant.

2.2.1. Posterior estimation. A reconstruction can be found by exploring the posterior distribution. Typically, the *maximum a posteriori* (MAP) estimate or the *conditional mean* (CM) estimate is computed. The corresponding estimation problems are defined as

$$\sigma_{\text{MAP}} = \arg\max_{\sigma\in\mathcal{A}} p(\sigma|\mathbf{V}) \qquad \text{and} \qquad \sigma_{\text{CM}} = \int_{\mathcal{A}} \sigma\, p(\sigma|\mathbf{V})\, \mathrm{d}\sigma. \tag{2}$$

Obtaining either of these can be a computationally challenging problem that requires the use of advanced optimization and numerical integration algorithms. Difficulties arise whenever the shape of the posterior distribution is such that the algorithms tend to proceed in wrong directions or get stuck around local maxima. In EIT reconstruction, these difficulties are caused by the nonlinearity and complexity of the forward map as well as by the ill-conditioned nature of the inverse problem.

2.3. Additive Gaussian noise model

In the model of additive Gaussian measurement noise, the noisy measurements $\mathbf{V}$ and the actual voltages on the electrodes $\mathbf{U}(\sigma)$ are assumed to be linked through the formula

$$\mathbf{V} = \mathbf{U}(\sigma) + \mathbf{N}, \tag{3}$$

where the noise term $\mathbf{N}$ is an independent Gaussian random variable with mean μ and covariance matrix Γ. This model specifies a likelihood of the form

$$p(\mathbf{V}|\sigma) = p_{\text{noise}}(\mathbf{V} - \mathbf{U}(\sigma)). \tag{4}$$

2.3.1. White noise model. This work uses what is here called the white noise model, where the measurement errors are assumed to be independent of each other, to have zero mean and a common *a priori* given variance, i.e. $\mu = 0$ and $\Gamma = \gamma_N^2 I$, where $\gamma_N^2 > 0$ is given. These are not fully realistic assumptions since in real life both μ and Γ involve some uncertainty. However, this model is used since it is typical that the covariance matrix is diagonal and the scale differences of the individual variances are not great [16].

2.3.2. Enhanced noise model. Suppose that the map $\sigma \to \widetilde{\mathbf{U}}(\sigma)$ is a simulation of the actual forward map $\sigma \to \mathbf{U}(\sigma)$ and that the forward simulation error $\mathbf{U}(\sigma) - \widetilde{\mathbf{U}}(\sigma)$ is not zero. In the enhanced noise model [17], *a priori* information about the forward simulation error is incorporated into the measurement error model. Formula (3) can be written as $\mathbf{V} = \widetilde{\mathbf{U}}(\sigma) + [\mathbf{U}(\sigma) - \widetilde{\mathbf{U}}(\sigma)] + \mathbf{N}$. Due to the forward simulation error, substituting $\widetilde{\mathbf{U}}(\sigma)$ directly into (3) can lead to errors in the reconstruction. In the enhanced noise model, the simulation and the actual measurements are assumed to be linked through the formula $\mathbf{V} = \widetilde{\mathbf{U}}(\sigma) + \widetilde{\mathbf{N}}$. The noise term $\widetilde{\mathbf{N}}$ is an independent Gaussian random variable with mean $\widetilde{\mu}$ and covariance matrix $\widetilde{\Gamma}$ of the form

$$\widetilde{\mu} = \int_{\mathcal{A}} [\mathbf{U}(\sigma) - \widetilde{\mathbf{U}}(\sigma)] p(\sigma)\, \mathrm{d}\sigma + \mu, \tag{5a}$$

$$\widetilde{\Gamma} = \int_{\mathcal{A}} [\mathbf{U}(\sigma) - \widetilde{\mathbf{U}}(\sigma) - \mu][\mathbf{U}(\sigma) - \widetilde{\mathbf{U}}(\sigma) - \mu]^{\top} p(\sigma)\, \mathrm{d}\sigma + \Gamma, \tag{5b}$$

where μ and Γ are the mean and covariance matrix of the actual measurement noise term in (3) respectively, and the integral terms are the conditional mean and the conditional covariance of the forward simulation error with respect to the prior density $p(\sigma)$.

3. Numerical methods

A finite dimensional representation of the reconstruction problem is obtained by applying the *finite element method* (FEM) [30]. The domain Ω is partitioned into a regular shape of a set of triangles $\mathcal{T}_h = \{T_1, T_2, \ldots, T_M\}$. The conductivity distribution is assumed to be spanned by characteristic functions of the triangles $T \in \mathcal{T}_h$, and the potential field in the domain is assumed to be spanned by n piecewise linear shape functions $\varphi_1, \varphi_2, \ldots, \varphi_n$ such that φ_k differs from zero precisely at the kth node of $\mathcal{T}_h$. The mesh parameter h is equal to half of the length of the longest edge in the triangulation.

3.1. Forward simulations

3.1.1. Standard FEM forward simulation. The map $\sigma \to \mathbf{U}_h(\sigma)$ denotes the standard FEM simulation of the actual forward map. Numerical evaluation of this map requires finding the FEM solution of the CEM equations with respect to each injected current pattern. Given a current pattern I, the FEM solution is

$$u_{\mathrm{FE}} = \sum_{i=1}^{N} \alpha_i \varphi_i \qquad \text{and} \qquad U_{\mathrm{FE}} = \sum_{i=1}^{L-1} \beta_i (\mathrm{e}_1 - \mathrm{e}_{i+1}),$$

where $\varphi_1, \varphi_2, \ldots, \varphi_N$ are the shape functions of the finite element space and $\mathrm{e}_1, \mathrm{e}_2, \ldots, \mathrm{e}_L$ are the standard basis vectors of $\mathbb{R}^L$. The coefficients $\alpha_1, \alpha_2, \ldots, \alpha_N$ and $\beta_1, \beta_2, \ldots, \beta_N$ can be found by solving an $(n + L - 1)$-dimensional symmetric and positive definite of the linear system of equations [31]

$$Ax = b, \tag{6}$$

where the entries of the vectors x and b are given by $x_i = \alpha_i$ and $b_i = 0$ respectively if $i \leqslant N$, otherwise $x_i = \beta_{i-N}$ and $b_i = (\mathrm{e}_1 - \mathrm{e}_{i+1-N})^T I$. The system matrix entries are given by

$$A_{i,j} = \begin{cases} B_{i,j} + C_{i,j} & \text{if} \quad i \leqslant N \text{ and } j \leqslant N, \\ -G_{i,1} + G_{i,j+1-N} & \text{if} \quad i \leqslant N \text{ and } j > N, \\ \dfrac{|e_1|}{z_1} + \delta_{i,j} \dfrac{|e_{j+1-N}|}{z_{j+1-N}} & \text{if} \quad i > N \text{ and } j > N, \end{cases}$$

where $B_{i,j} = \int_\Omega \sigma \nabla\varphi_i \cdot \nabla\varphi_j \,\mathrm{d}x\,\mathrm{d}y$, $C_{i,j} = \sum_{\ell=1}^{L} \frac{1}{z_\ell} \int_{e_\ell} \varphi_i \varphi_j \,\mathrm{d}s$, $G_{i,j} = \frac{1}{z_j} \int_{e_j} \varphi_i \,\mathrm{d}s$, $|e_i| = \frac{1}{z_i} \int_{e_i} \mathrm{d}s$, and $\delta_{i,j}$ is the Kronecker delta.

Since in this study only a relatively small anomaly is sought, the linear system (6) can be solved using the Sherman–Morrison–Woodbury formula [12, 16]. This provides a way to make low-rank updates to a matrix inverse with a low computational cost.

3.1.2. Linearized FEM forward simulation. For some purposes, the FEM solution can be computationally too expensive to be used in the reconstruction procedure. In such a case, one can use e.g. a linearization of the form:

$$\mathbf{U}_{ln}(\sigma) = \mathbf{U}_h(\sigma_0) + D\mathbf{U}_h(\sigma_0)(\sigma - \sigma_0), \tag{7}$$

where the linearization point σ_0 is some properly chosen initial conductivity distribution and $D\mathbf{U}_h(\sigma_0)$ is the Jacobian matrix [16] of $\mathbf{U}_h(\sigma)$ evaluated at σ_0. It is often computationally cheaper to numerically evaluate $\mathbf{U}_{ln}(\sigma)$ than $\mathbf{U}_h(\sigma)$. It is, however, also possible that the accuracy of (7) is inadequate for EIT reconstruction since it is not always possible to choose a good enough initial conductivity distribution.

3.2. Prior densities

3.2.1. Anomaly prior. In the implemented anomaly prior, it is assumed that the conductivity distribution is of the form

$$\sigma = \sigma_{\mathrm{bg}} + \sigma_{\mathrm{an}}, \tag{8}$$

where σ_{bg} is a background conductivity and σ_{an} is an anomalous conductivity that obtains the value t in a disc of radius r centred at (c_1, c_2) and is zero everywhere else. With this assumption, there is a bijective correspondence between σ and

$$\hat{\sigma} = (c_1, c_2, r, t). \tag{9}$$

It is assumed that $\hat{\sigma}$ is uniformly distributed over the four-dimensional rectangular set in which

$$\hat{\sigma}_{\min} \preceq \hat{\sigma} \preceq \hat{\sigma}_{\max}.$$

Here, the symbol $\preceq$ denotes that all the components on the left-hand side are less than or equal to the components on the right-hand side. If this set is small enough, this prior can be regarded as informative.

Possible real-life applications in which this prior may be used are the detection of a tumour in breast tissue as a medical application and the detection of a particle in a fluid-filled tank as an industrial one. Note that in numerical implementation of this prior, anomalous conductivities (8) have to be interpolated into the mesh in which the inverse problem is solved. This work uses a piecewise constant interpolation in which the interpolant is constant on each triangle in $\mathcal{T}_h$ and the circumcentres of the triangles are the interpolation points.

3.2.2. Smoothness prior. The smoothness prior applied in this work is a Gaussian prior of the form $p(\sigma) \propto \exp(-\sigma^T \Gamma^{-1} \sigma)$, where Γ^{-1} is a system matrix of a FEM discretized Laplace's equation with zero boundary conditions. A Delaunay triangulation, i.e. a triangulation such that no data points are contained in any triangle's circumcircle, is used in the construction of the covariance matrix. Nodes of the Delaunay triangulation are the set of circumcentres of $\mathcal{T}_h$, and the corresponding piecewise linear shape functions are denoted by $\phi_1, \phi_2, \ldots, \phi_M$. If the

minimum distance from the support of $\phi_i + \phi_j$ to the boundary $\partial\Omega$ is greater than or equal to the mesh parameter h, then

$$\Gamma^{-1}_{i,j} = \int_\Omega \nabla\phi_i \cdot \nabla\phi_j \, \mathrm{d}x \, \mathrm{d}y,$$

otherwise $\Gamma^{-1}_{i,j} = \delta_{i,j}$, i.e. the submatrix corresponding to the triangles near the boundary is an identity matrix.

As a Gaussian prior this smoothness prior is differentiable. Differentiability of the prior is necessary in quasi-Newton optimization. In contrast, priors that allow moderate discontinuities in conductivities, e.g. the above-described anomaly prior, are non-differentiable [16].

3.3. Reconstruction methods

3.3.1. Quasi-Newton optimization. In the following quasi-Newton (Gauss–Newton) algorithm, a MAP estimate is found by approximately minimizing the posterior density proportional to the negative exponent of

$$\Phi(\sigma|\mathbf{V}) = \tfrac{1}{2}[\mathbf{V} - \mathbf{U}(\sigma)]^\top \Gamma^{-1}[\mathbf{V} - \mathbf{U}(\sigma)] + \alpha\Psi(\sigma). \tag{10}$$

Here, the negative exponent of $\frac{1}{2}[\mathbf{V} - \mathbf{U}(\sigma)]^\top \Gamma^{-1}[\mathbf{V} - \mathbf{U}(\sigma)]$ is proportional to the likelihood and the negative exponent of $\alpha\Psi(\sigma)$ defines a regularizing prior (here the smoothness prior), up to a constant factor. Connection to classical regularization is obvious; the global minimizer of the function $\Phi(\sigma|\mathbf{V})$ is also known as a regularized least-squares solution of the reconstruction problem.

Algorithm 3.1. *The quasi-Newton algorithm*

- *Choose an initial guess* $\sigma^{(0)}$*, a relaxation parameter* $0 < \lambda \leqslant 1$*, and* $N \geqslant 1$*. For* $i = 0, 1, \ldots, N-1$*, repeat the following two steps:*
- *calculate the gradient of* $\Phi(\cdot|\mathbf{V})$ *and its Jacobian matrix at* $\sigma^{(i)}$*:*

$$\nabla\Phi(\sigma^{(i)}|\mathbf{V}) = D\mathbf{U}(\sigma^{(i)})^\top \Gamma^{-1}[\mathbf{V} - \mathbf{U}(\sigma^{(i)})] + \alpha D\Psi(\sigma^{(i)}),$$

$$D\nabla\Phi(\sigma^{(i)}|\mathbf{V}) = D\mathbf{U}(\sigma^{(i)})^\top \Gamma^{-1} D\mathbf{U}(\sigma^{(i)}) + \alpha D^2\Psi(\sigma^{(i)}).$$

- *Calculate the next state as*

$$\sigma^{(i+1)} = \sigma^{(i)} - \lambda[D\nabla\Phi(\sigma^{(i)}|\mathbf{V})]^{-1}\nabla\Phi(\sigma^{(i)}|\mathbf{V}).$$

This algorithm relies on the assumption that $\Psi(\sigma)$ is differentiable as well as on the assumption that the initial guess is good enough.

It is typical that only one step of this algorithm is applied [16]. In such a case, a linearized solution of the MAP estimation problem, given in (2), is obtained.

3.3.2. Markov chain Monte Carlo sampling. The so-called Monte Carlo estimate [20] of the conditional mean σ_{CM}, given in (2), is the left-hand side of

$$\sigma_{\mathrm{CM}} \approx \frac{1}{m}\sum_{i=1}^{m} \sigma^{(i)},$$

where $\{\sigma^{(i)}\}_{i=1}^{\infty}$ is an ergodic Markov chain with invariant density $p(\sigma|\mathbf{V})$. Convergence of the estimate follows from the law of large numbers and the central limit theorem for ergodic Markov chains [22]. According to the central limit theorem, the estimation error is asymptotically Gaussian with zero mean and covariance matrix that tends to zero at the rate

$O(1/m)$. The goal in Markov chain Monte Carlo sampling is to produce an ergodic Markov chain such that a reasonable convergence rate is achieved in practice. The rate of convergence in terms of CPU time is affected by several factors, such as complexity of the applied sampling strategy.

Since in EIT reconstruction the dependence of the noiseless voltage data on the conductivity distribution is highly nonlinear, it is difficult to determine a decent approximation for the posterior. The following simple random-walk Metropolis algorithm is adopted in this study since it is a common choice when the shape of the posterior is not known [20].

Algorithm 3.2. *The random-walk Metropolis*

- *Given are the current state $\sigma^{(i)}$ and the proposal variance $\gamma^2 > 0$.*
- *Pick a random perturbation ε from a Gaussian distribution with zero mean and covariance matrix $\gamma^2 I$, and propose a move $\xi = \sigma^{(i)} + \varepsilon$.*
- *Pick a uniformly distributed random number t between 0 and 1 and set*

$$\sigma^{(i+1)} = \begin{cases} \xi & \text{if } t \leqslant p(\xi|\mathbf{V})/p(\sigma^{(i)}|\mathbf{V}), \\ \sigma^{(i)} & \text{otherwise.} \end{cases}$$

The proposal variance should be chosen so that the acceptance rate, i.e. the ratio of accepted and proposed moves, is relatively close to 0.234, which is according to Roberts *et al* [26] the asymptotically optimal acceptance rate under quite general conditions.

3.3.3. Two-stage reconstruction. The two-stage reconstruction process investigated in this paper is a combination of the above-described numerical methods. In the first stage, a MAP estimate is produced by applying one step of algorithm 3.1 in which the smoothness prior is used as the regularizing prior. Then, a region of interest $\mathcal{R}$ potentially containing the anomaly is determined through

$$\mathcal{R} = \{x \in \Omega : |\sigma(x) - \sigma_{\text{bg}}(x)| \geqslant \kappa \ \text{std}(\sigma)\}, \tag{11}$$

where σ is the MAP estimate, $\text{std}(\sigma)$ is its standard deviation and $\kappa > 0$ is a thresholding parameter. In the second stage, an anomaly prior is chosen based on the set $\mathcal{R}$, and algorithm 3.2 is employed in exploration of the corresponding posterior.

The reconstruction process is split into two stages, since on one hand, MCMC sampling speed can be substantially increased if the ROI is given, and on the other hand, quasi-Newton optimization provides a computationally cheap way to determine the ROI. The resulting reconstruction strategy is, however, not fully Bayesian since the ROI determined in the first stage is used as *a priori* information in the second stage. Rather, it is a bootstrap approach to Bayesian inversion. Construction of a bootstrap prior from a robust reconstruction has been suggested by Calvetti and Somersalo [5].

4. Numerical experiments

This section reports numerical experiments in which a circular anomaly (e.g. a tumour in breast tissue) was sought from a polygonal approximation of the unit disc using the two-stage reconstruction. The computations were performed using MATLAB 6.5 software and 1.3 GHz Celeron M 350 notebook with 512Mb RAM.

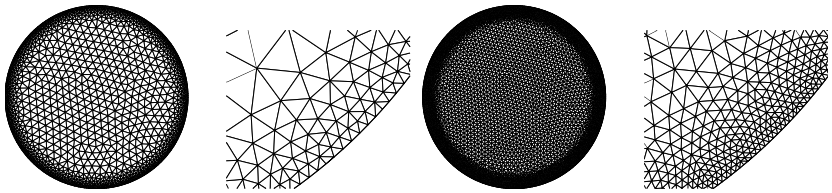

Figure 1. The triangulation $\mathcal{T}_h$ (left) and the refined mesh $\mathcal{T}_{h/2}$ (right). The former was used in the reconstruction procedure and the latter was used in simulation of the measurement data $\mathbf{V}$.

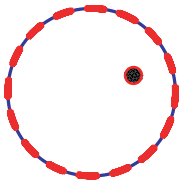

Figure 2. The anomaly sought (e.g. a tumour in breast tissue). The dashed red circle shows the size and the location.

4.1. Setup

In the computations, the domain Ω was a polygonal approximation of the unit disc. Sixteen electrodes ($L = 16$) were placed evenly on the boundary $\partial\Omega$. Together they cover 50% of the total boundary length. The contact impedances $z_1, z_2, \ldots, z_L$ were assumed to be equal to 1. The triangulation $\mathcal{T}_h$ consisted of 1476 nodes, 2659 triangles and 291 boundary edges (figure 1). The triangulation was refined towards $\partial\Omega$ since the potential distribution is not smooth on $\partial\Omega$. Namely, the boundary conditions of the forward problem (1) imply discontinuity of $\partial u/\partial n$ on $\partial\Omega$.

The voltage data were gathered by applying trigonometric current patterns $I_\ell^{(k)}$, $\ell = 1, 2, \ldots, L-1$ given by

$$I_\ell^{(k)} = \begin{cases} \cos(k\theta_\ell), & k = 1, 2, \ldots, L/2, \\ \sin((k - L/2)\theta_\ell), & k = L/2, L/2+1, \ldots, L-1, \end{cases}$$

where $\theta_\ell = 2\pi\ell/L$ is the angular location of the midpoint of the electrode e_ℓ. According to Cheney and Isaacson [6, 15], this is an optimal way to distinguish a centred rotation invariant annulus from a homogenous disc.

The anomalous conductivity distribution (figure 2) to be reconstructed from the noisy measurement data was a piecewise constant interpolant of

$$\hat{\sigma}_{\text{ex}} = (0.5, 0.2, 0.1, 0.1).$$

The interpolation points were the circumcentres of a refined triangulation $\mathcal{T}_{h/2}$ illustrated in figure 1. The refined triangulation was constructed by dividing each triangle in $\mathcal{T}_h$ into four subtriangles.

4.2. Simulated measurement data

The simulated noiseless electrode voltage vector $\mathbf{U}(\sigma_{ex})$ was obtained by finding the finite element solution of the forward problem with respect to the piecewise linear nodal basis of $\mathcal{T}_{h/2}$. The simulated measurement vector $\mathbf{V}$ was generated by adding Gaussian white noise $\mathbf{N}$

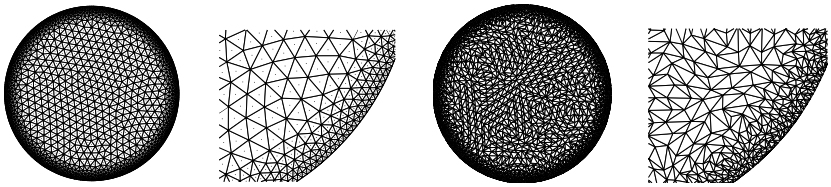

Figure 3. The circumcentres of the triangulation $\mathcal{T}_h$ (left) which form the nodes of the Delaunay triangulation (right).

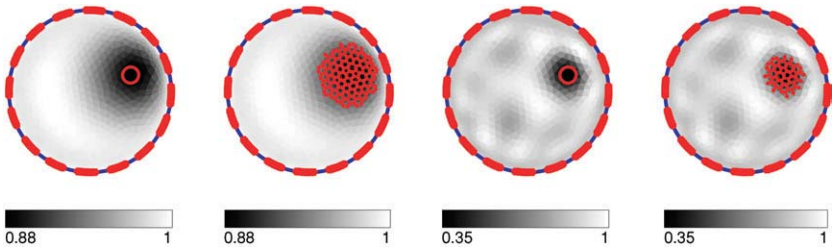

Figure 4. Quasi-Newton reconstructions corresponding to $\alpha = 10^{-1}$ (first from the left) and $\alpha = 10^{-5}$ (third). In both cases, the region of interest denoted by the red points is determined as described in (11) with $\kappa = 2.2$ (second and fourth).

with zero mean and covariance matrix $\Gamma = 10^{-6}I$ to the noiseless electrode potential values. This corresponds to a measurement error of the order

$$\|\mathbf{N}\|_2/\|\mathbf{U}(\sigma_{\text{ex}}) - \mathbf{U}(\sigma_{\text{bg}})\|_2 \approx 5\%. \tag{12}$$

The data were generated using a refined mesh, since otherwise the forward simulation error would have been zero, which is not realistic. Using the same mesh in both generating the data and solving the inverse problem is a so-called inverse crime. The forward simulation error was

$$\|\mathbf{U}_h(\sigma_{\text{bg}}) - \mathbf{U}(\sigma_{\text{bg}})\|_2/\|\mathbf{U}(\sigma_{\text{ex}}) - \mathbf{U}(\sigma_{\text{bg}})\|_2 \approx 29\%. \tag{13}$$

4.3. First reconstruction stage (quasi-Newton optimization)

In the first stage of the two-stage reconstruction process, a MAP estimate was computed by applying one step of algorithm 3.1. The background conductivity distribution σ_{bg} was used as the initial guess. The parameter λ controlling the step size was chosen to be 1. The white noise model and the smoothness prior were applied in the reconstruction process. In the white noise model, the actual mean and covariance matrix of the measurement noise, $\mu = 0$ and $\Gamma = 10^{-6}I$, were assumed to be given. The Delaunay triangulation applied in the construction of the smoothness prior is illustrated in figure 3. The gradient and the Jacobian matrix of the maximized function $\Phi(\sigma|\mathbf{V})$ were computed by using the standard FEM forward simulation.

4.3.1. Results. The obtained MAP estimates give information about the location of the anomaly, but not about its radius or its value of conductivity. Two reconstructions corresponding to two different regularization parameter values $\alpha = 10^{-1}$ and $\alpha = 10^{-5}$ are shown in figure 4. Decreasing the value of the regularization parameter led not only to better localization of the anomaly but also to an increased level of the overall variation of the reconstruction. The regions of interest illustrated in figure 4 were determined as described

Table 1. Three different anomaly priors.

	Lower bounds ($\hat{\sigma}_{\min}$)				Upper bounds ($\hat{\sigma}_{\max}$)			
Prior	c_1	c_2	r	t	c_1	c_2	r	t
(a)	0.35	0.05	0.05	0.01	0.65	0.25	0.25	1.00
(b)	0.35	0.05	0.10	0.01	0.65	0.25	0.10	1.00
(c)	0.35	0.05	0.05	0.10	0.65	0.25	0.25	0.10

Table 2. The applied prior, the noise model, the forward simulation method, the total number of steps, the length of the burn-in sequence, the number of steps between retained samples, the proposal standard deviation (PSD) and the acceptance rate (AR) in the five executed sampling runs.

Run	Prior	Noise	FEM	Steps	Burn-in	Ret.[a]	PSD[b]	AR[c]
(i)	(a)	White	Standard	100 000	2000	9	0.034	0.24
(ii)	(b)	White	Standard	100 000	2000	9	0.080	0.24
(iii)	(c)	White	Standard	100 000	2000	9	0.025	0.24
(iv)	(b)	White	Linearized	100 000	2000	9	0.020	0.23
(v)	(b)	Enhanced	Linearized	100 000	2000	9	0.075	0.23

[a] Number of steps between retained samples.
[b] Proposal standard deviation.
[c] Acceptance rate.

in (11) with the choice $\kappa = 2.2$ for the thresholding parameter. Performing one step of the algorithm took about 15 s of CPU time.

4.4. Second reconstruction stage (MCMC sampling)

In the second reconstruction stage, a conditional mean estimate was computed by employing algorithm 3.2. The anomaly prior was applied based on three different *a priori* assumptions (a), (b) and (c), as listed in table 1. In the prior (a), all the variables c_1, c_2, r and t are assumed to be unknown. The true value of r is given in (b) and the true value of t is given in (c). The first prior represents the general case. The two latter priors can be used e.g. in industrial applications where the particle size or the particle conductivity can be given.

The executed MCMC runs (i)–(v) are listed in table 2. The state space of the Markov chain was four dimensional in the sampling run (i) and three dimensional in runs (ii)–(v). In each run, the proposal variance, i.e. the variance of the random error ε, was chosen so that the acceptance rate is close to the asymptotically optimal value 0.234 [26]. All the sampling runs were of length 100 000 steps. The first 2000 steps were discarded as a burn-in sequence. A simple blocking strategy was applied by retaining only every tenth step of the iteration as a sample. Consequently, the total number of samples generated in one run was 9800. Based on each individual sampling run, a conditional mean estimate (9) was computed.

The standard and linearized FEM forward simulations were applied to the reconstruction process. In the numerical evaluation of $\mathbf{U}_h(\sigma_{\text{an}})$, the electrode potential vector $\mathbf{U}_h(\sigma_{\text{bg}})$ was updated using the Sherman–Morrison–Woodbury formula [12, 16], which performs well due to the relatively small size of the anomaly. Two noise models were used, namely, the white noise model and the enhanced noise model. The actual mean and covariance matrix of the measurement noise, $\mu = 0$ and $\Gamma = 10^{-6} I$, were assumed to be given. Estimates of the integral terms in (5*a*) and (5*b*) were computed as Monte Carlo estimates from 1000 independent random draws from the prior (a). In the numerical evaluation of the integrands, the standard FEM forward simulation was used.

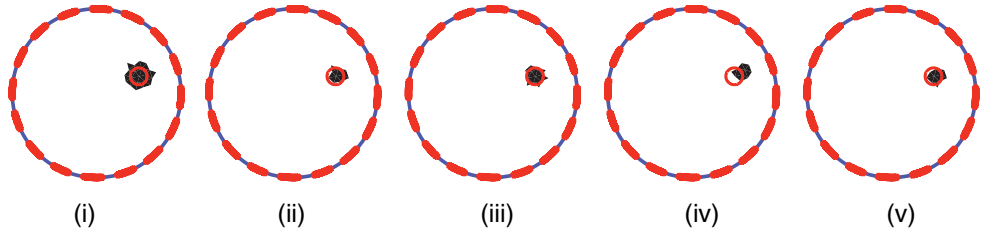

Figure 5. Monte Carlo estimates of the conditional mean after 100 000 iterations in the sampling runs (i)–(v). The (red) circle shows the exact size and shape of the anomaly. A correct location but a clearly wrong size was found in the run (i). Runs (ii) and (iii) produced the best reconstructions. The anomaly was located incorrectly in the run (iv) in which the linearized FEM forward simulation and the white noise model were applied. A better location was found in the run (v), where in contrast, the enhanced noise model was used together with the linearized FEM simulation.

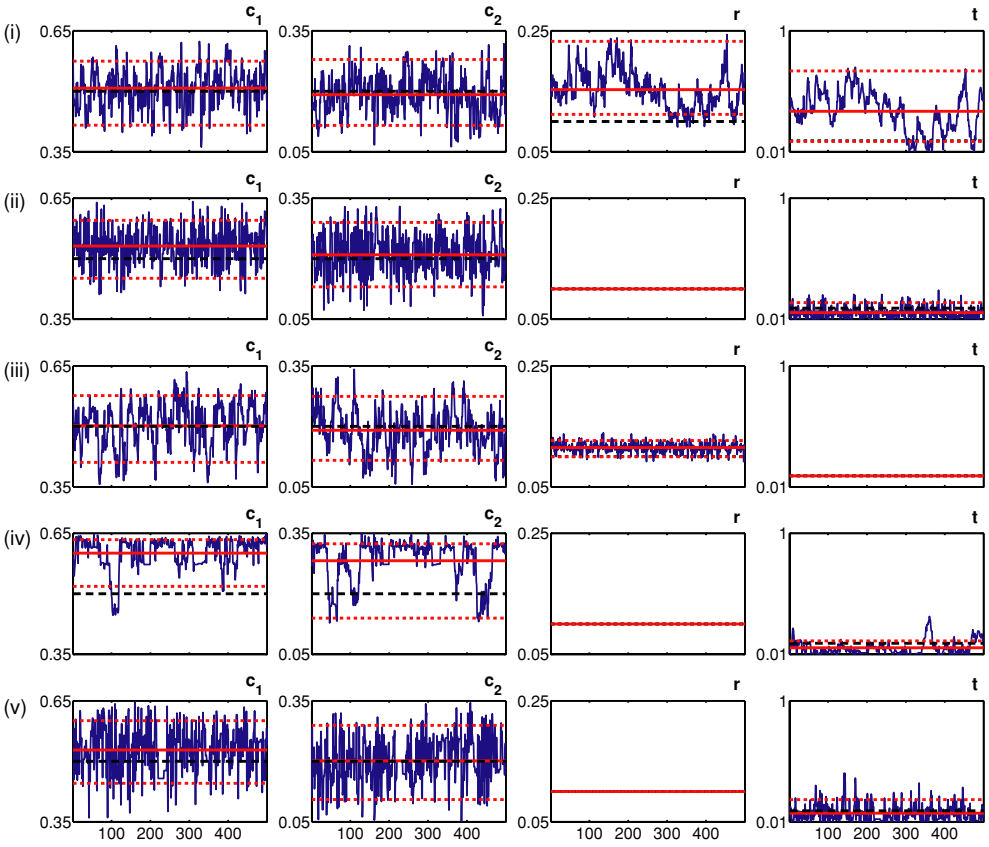

Figure 6. The first 500 iteration steps after the burn-in sequence in cases (i)–(v). Behaviour of the variables c_1 (1st column), c_2 (2nd column), r (3rd column) and t (4th column) is illustrated in separate figures. The dashed black line indicates the true value, the solid (red) line shows the Monte Carlo approximation and the two dotted (red) lines show the 90% credible interval.

4.4.1. Results. The results of the executed sampling runs are reported in figures 5–7. These show that in the case (i), the true values of t and r were not found due to the ill-conditioned nature of the inverse problem and due to the high correlation between these variables. Correlation

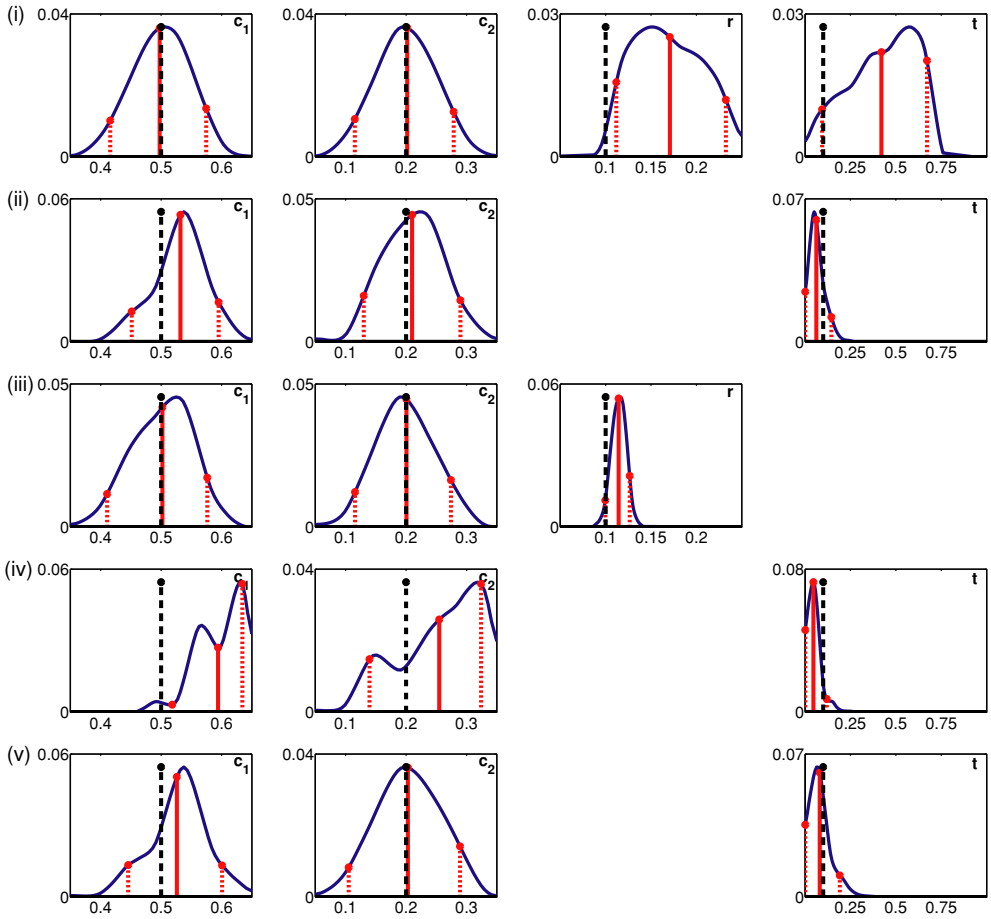

Figure 7. Marginal densities in cases (i)–(v). Marginal densities of the variables c_1 (1st column), c_2 (2nd column), r (3rd column) and t (4th column) are illustrated in separate figures. The dashed black stem indicates the true value. The solid (red) stem shows the conditional mean and the two dotted (red) stems show the 90% credible interval.

Table 3. Correlation of the variables c_1, c_2, r and t in the sampling run (i).

	Correlation coefficients			
	c_1	c_2	r	t
c_1	1.00	−0.01	−0.15	−0.01
c_2	−0.01	1.00	−0.07	−0.02
r	−0.15	−0.07	1.00	0.94
t	−0.01	−0.02	0.94	1.00

coefficients between the variables c_1, c_2, r and t in the sampling run (i) are reported in table 3. Fairly good reconstructions were obtained in cases (ii) and (iii) in which either r or t is fixed to its true value. The anomaly was clearly dislocated in the case (iv) where the posterior density was evaluated numerically using the linear FEM forward simulation. A better location was found in the sampling run (v) which differs from (iv) only by the noise model. Execution time was between 6 and 7 min in runs (i)–(iii) and between 13 and 14 min in runs (iv) and (v).

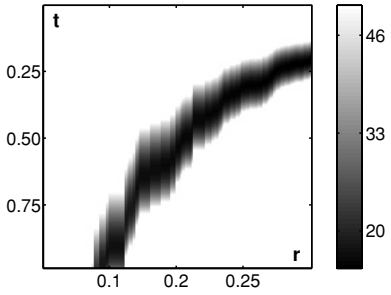

Figure 8. A pseudocolour plot of the absolute value of the natural logarithm of the likelihood function $p(\mathbf{V}|\sigma)$, evaluated numerically using the standard FEM forward simulation. Here, the centre point of the anomaly (c_1, c_2) is fixed to its true value (0.5, 0.2), and the radius r (horizontal axis) and the value of t (vertical axis) are varied. The darkened part of the image shows where the absolute value of the natural logarithm of the likelihood is less than 50.

5. Discussion

Numerical experiments, in which a circular anomaly was sought from a polygonal approximation of the unit disc using the two-stage reconstruction, were reported in this paper. The performances of two different additive Gaussian noise models were compared. The first was the white noise model, where the measurement errors were assumed to be independent of each other and to have zero mean. The second was the enhanced noise model proposed by Kaipio and Somersalo [17], which incorporates *a priori* information about the errors in forward modelling. The forward model considered in this study was the CEM by Somersalo *et al* [28]. In the numerical experiments, the CEM was simulated using the FEM [30]. Performances of standard [31] and linearized FEM forward simulations were compared.

In the first reconstruction stage, the implemented quasi-Newton algorithm provided a computationally cheap but robust MAP estimate. However, based on the present numerical results concerning two-stage reconstruction, it is suggested that using a reconstruction produced by the quasi-Newton algorithm one can construct an (bootstrap) anomaly prior to be used in the second reconstruction stage.

In the second reconstruction stage, the implemented random-walk algorithm produced very accurate reconstructions in the sampling runs (ii), (iii) and (v), but failed to find the correct values of r and t in the sampling run (i) and the correct values of c_1 and c_2 in the sampling run (iv).

The reason for the failure in the run (i) is that the posterior distribution does not have a unique minimum because it is 'banana-shaped' in an rt-plane as illustrated in figure 8. This also means that r and t are highly correlated variables. It is obvious that a better sampling strategy should be developed. Firstly, it is a commonly observed problem that the random-walk algorithm does not perform well in cases of correlated variables since the proposal tends to waste effort exploring the distribution in wrong directions. Secondly, the random walk gets easily stuck around the local maxima if the random-walk steps are not restricted to the ROI. Consequently, the random walk is likely to find ghost anomalies if it is allowed to move all around the domain. Monte Carlo methodology involves various sophisticated sampling schemes [20, 25], e.g. the Metropolis-adjusted Langevin algorithm, that may perform better than the random-walk Metropolis, especially in cases where the background conductivity distribution is not constant.

It is also important to point out that the forward simulation error (13) is large compared to the measurement error (12). Refining the triangulation would reduce the forward simulation

error and lead to better reconstructions. However, each triangulation has its maximal resolution. For any triangulation, there are anomalies for which the forward simulation error is large. This study considered the case in which the anomaly is small in terms of resolution of the triangulation. Another topic would be to examine the case where the measurement error is the dominant one. This will require rigorous forward modelling. In such a study, accurate numerical methods for elliptic boundary value problems and the high-order finite element method (hp-FEM) [24, 30] can be applied.

The reason for the failure in sampling run (iv) is the combination of the linearized FEM forward simulation and the white noise model. In this study, the standard FEM forward simulation was applicable because the conductivity updates are small and restricted to the ROI. Since computational cost in the numerical evaluation of the map $\sigma \to \mathbf{U}_{ln}(\sigma)$ is independent of the structure of the conductivity distribution, it is important to study whether it would be advantageous to use the linearized FEM forward simulation in the sampling process. A comparison of the sampling runs (ii) and (iv), however, shows that the use of the linearized FEM forward simulation leads to less accurate reconstructions than the use of the standard FEM forward simulation. In the sampling run (iv), the anomaly is dislocated even though its size is given. A comparison of runs (iv) and (v) shows that the performance of the enhanced noise model is superior to the white noise model when the linearized FEM forward simulation is used.

6. Summary and conclusions

The findings and conclusions of this study supporting the applicability of two-stage reconstruction of circular anomalies in EIT are as follows.

- The investigated two-stage reconstruction process can be applied in the detection of circular anomalies.
- A smoothness prior can be constructed effectively using the finite element method as described in section 3.2.2.
- An anomaly prior can be constructed using the c_1, c_2, r, t coordinates and the piecewise constant interpolation scheme introduced in section 3.2.1.
- The standard FEM forward simulation performance is superior to the linearized FEM forward simulation.
- The enhanced noise model performance is superior to that of the white noise model when linearized FEM forward simulation is used.
- Future work could involve more sophisticated MCMC sampling as well as rigorous forward simulation using the hp-FEM.

References

[1] Ammari H, Beretta E and Francini E 2004 Reconstruction of thin conductivity imperfection *Appl. Anal.* **83** 63–76

[2] Andersen K E, Brooks S P and Hansen M B 2001 A Bayesian approach to crack detection in electrically conducting media *Inverse Problems* **17** 121–36

[3] Beretta E, Francini E and Vogelius M 2003 Asymptotic formulas for steady state voltage potentials in the presence of thin inhomogeneities. A rigorous error analysis *J. Math. Pures Appl.* **82** 1277–301

[4] Calderon A P 1980 On an inverse boundary value problem *Seminar on Numerical Analysis and its Applications to Continuum Physics* (Rio de Janeiro: Soc. Brasil. Mat.) pp 65–73

[5] Calvetti D and Somersalo E 2005 Bayesian image deblurring and boundary effects *Advanced Signal Processing Algorithms, Architecture and Implementations XV, Proc. SPIE* vol 5910 (Bellinghan WA: SPIE Optical Engineering Press) p 59100X-1

[6] Cheney M and Isaacson D 1992 Distinguishability in impedance imaging *IEEE Trans. Biomed. Eng.* **39** 852–60
[7] Cheney M, Isaacson D and Newell J C 1999 Electrical impedance tomography *SIAM Rev.* **41** 85–101
[8] Cherepenin V A, Karpov A Y, Korjenevsky A V, Kornienko V N, Kultiasov Y S, Ochapkin M B, Trochanova O V and Meister J D 2002 Three-dimensional EIT imaging of breast tissues: system design and clinical testing *IEEE Trans. Med. Imaging* **21** 662–7
[9] Clay M T and Ferree T C 2002 Weighted regularization in electrical impedance tomography with applications to acute cerebral stroke *IEEE Trans. Med. Imaging* **21** 629–37
[10] Dickin F and Wang M 1996 Electrical resistance tomography for process applications *Meas. Sci. Technol.* **7** 247–60
[11] Fox C and Nicholls G K 1997 *Sampling conductivity images via MCMC Proceedings of the Leeds Annual Statistical Research Workshop (LASR)* vol 1 (Leeds: Leeds University Press) p 91
[12] Golub G and van Loan C 1989 *Matrix Computations* (Baltimore: The John Hopkins University Press)
[13] Hartov A, Soni N K and Paulsen K D 2004 Variation in breast EIT measurements due to menstrual cycle *Physiol. Meas.* **25** 295–9
[14] Heikkinen L M, Leinonen K, Kaipio J P, Vauhkonen M and Savolainen T 2001 Electrical process tomography with known internal structures and resistivities *Inverse Problems* **9** 431–54
[15] Isaacson D 1993 Distinguishability of conductivities by electric current computed tomography *IEEE Trans. Biomed. Eng.* **40** 1328–30
[16] Kaipio J P, Kolehmainen V, Somersalo E and Vauhkonen M 2000 Statistical inversion and Monte Carlo sampling methods in electrical impedance tomography *Inverse Problems* **16** 1487–522
[17] Kaipio J P and Somersalo E 2004 *Statistical and Computational Methods for Inverse Problems* (Berlin: Springer)
[18] Kaup P G, Santosa F and Vogelius M 1996 Method for imaging corrosion damage in thin plates from electrostatic data *Inverse Problems* **12** 279–93
[19] Kerner T E, Paulsen K D, Hartov A, Soho S K and Poplack S P 2002 Electrical impedance spectroscopy of the breast: clinical imaging results in 26 subjects *IEEE Trans. Med. Imaging* **21** 638–45
[20] Liu J S 2001 *Monte Carlo Strategies in Scientific Computing* (Berlin: Springer)
[21] Mueller J L, Isaacson D and Newell J C 1999 A reconstruction algorithm for electrical impedance tomography data collected on rectangular electrode arrays *IEEE Trans. Biomed. Eng.* **46** 1379–86
[22] Nummelin E 1984 *General Irreducible Markov Chains and Non-Negative Operators* (Cambridge: Cambridge University Press)
[23] Polydorides N, Lionheard W R B and McCann H 2002 Krylov subspace iterative techniques: on the detection of brain activity with electrical impedance tomography *IEEE Trans. Med. Imaging* **21** 596–603
[24] Pursiainen S and Hakula H 2006 A high-order finite element method for electrical impedance tomography *Progress in Electromagnetics Research Symp. 2006 Cambridge Proc.* vol 1 (Cambridge, MA: The Electromagnetics Academy) p 260
[25] Robert C P and Casella G 1999 *Monte Carlo Statistical Methods* (New York: Springer)
[26] Roberts G O, Gelman A and Gilks W R 1997 Weak convergence and optimal scaling for random walk Metropolis algorithms *Ann. Appl. Probab.* **7** 110–20
[27] Seppänen A, Heikkinen L M, Savolainen T, Somersalo E and Kaipio J P 2003 An experimental evaluation of state estimation with fluid dynamical models in process tomography *Proc. 3rd World Congress on Industrial Process Tomography* vol 1 p 541
[28] Somersalo E, Cheney M and Isaacson D 1992 Existence and uniqueness for electrode models for electric current computed tomography *SIAM J. Appl. Math.* **52** 1023–40
[29] Stanley S J, Mann R and Primrose K 2002 Tomographic imaging of fluid mixing in 3D for single-feed semi-batch operation of a stirred vessel *Chem. Eng. Res. Des.* A **80** 903–9
[30] Szabo B and Babuska I 1991 *Finite Element Analysis* (New York: Wiley)
[31] Vauhkonen M 1997 Electrical impedance tomography and prior information *PhD Thesis* University of Kuopio, Kuopio, Finland
[32] Vilhunen T, Heikkinen L M, Savolainen T, Vauhkonen P J, Lappalainen R, Kaipio J P and Vauhkonen M 2002 Detection of faults in resistive coatings with an impedance-tomography-related approach *Meas. Sci. Technol.* **13** 865–72
[33] Wang W, Tang M, McCormick M and Dong X 2001 Preliminary results from an EIT breast imaging simulation system *Physiol. Meas.* **22** 39–48